

Design and fabrication of a glass waveguide optical add-drop multiplexer by use of an amorphous-silicon overlay distributed Bragg reflector

Jaeyoun Kim, Guangyu Li, and Kim A. Winick

We report the fabrication of a distributed Bragg reflector (DBR) on a silver ion-exchanged glass waveguide with a patterned overlay of sputter-deposited amorphous silicon (a-Si). Using this high-refractive-index overlay DBR technology, we demonstrate a fully functional glass-integrated optic add-drop multiplexer (OADM). The OADM consists of a Mach-Zehnder interferometer (MZI) containing overlay DBR gratings in both arms. The design, fabrication, and characterization procedures of the sputter-deposited a-Si overlay DBR and the ion-exchanged glass waveguide MZI are discussed in detail. The completed 3-cm-long OADM exhibited a 24-dB transmission dip with a 3-dB bandwidth of 0.5 nm. The 1-cm-long a-Si overlay DBR induced an additional attenuation of 1.2 dB. A simplified method for overlay DBR fabrication that utilizes a lift-off technique is also proposed and demonstrated. © 2004 Optical Society of America

OCIS codes: 130.0130, 130.3120, 310.0310, 310.1860, 060.1810, 060.4230.

1. Introduction

In this paper we demonstrate use of a patterned amorphous-silicon overlay to realize efficient distributed Bragg reflector (DBR) gratings on an ion-exchanged glass substrate. To date DBR gratings have been fabricated primarily by direct surface corrugation of the substrate¹ or by UV writing in high-silica glasses.² There are situations, however, where neither method is appropriate. The patterned high-refractive-index overlay technique discussed here was originally proposed by Hussell and Ramaswamy³ for producing surface-corrugated DBRs on hard-to-etch substrates such as LiNbO₃. Many multicomponent ion-exchangeable glass substrates, however, are also difficult to etch and do not exhibit much UV sensitivity. Thus the overlay DBR technique has wide applicability. Some high-index overlay materials such as silicon show enhanced

electro-optic,⁴ thermo-optic,⁵ and nonlinear optical⁶ properties that may also be exploited to increase device functionality. We previously utilized a plasma-enhanced chemical vapor deposition (PECVD) amorphous-silicon DBR overlay to implement a glass waveguide DBR laser in potassium ion-exchanged Er/Yb co-doped phosphate glass.⁷ In this paper the amorphous silicon is deposited by sputtering rather than PECVD to accommodate the low-temperature requirements associated with silver ion-exchange waveguides.

Recent advances in wavelength-division multiplex systems have motivated development of integrated optical add-drop multiplexers (OADMs) based on four-port, Mach-Zehnder interferometer (MZI) structures.⁸ Figure 1 shows schematically the basic structure and operational principles of the MZI OADM. When an optical signal, with its wavelength located within the DBR bandwidth, enters the device from port A, it sequentially experiences a 3-dB power split at the directional coupler (DC) #1, reflection by the DBR, recombination back at DC#1, and finally exits the device (dropped) from port B. Optical signals that lie outside the DBR bandwidth passes through the MZI and exits the OADM from port D. Kashyap *et al.*² reported the first integrated-optic implementation of the MZI OADM with UV-

The authors are with the Department of Electrical Engineering and Computer Science, The University of Michigan, Ann Arbor, Michigan 48109-2122.

Received 14 May 2003; revised manuscript received 26 September 2003; accepted 29 September 2003.

0003-6935/04/030671-07\$15.00/0

© 2004 Optical Society of America

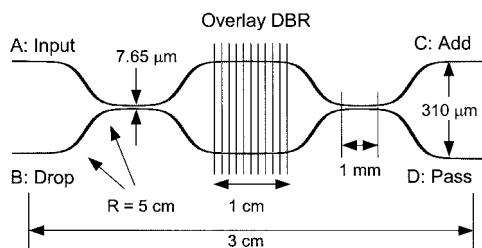


Fig. 1. Schematic view of an OADM based on the MZI structure.

written gratings on Ge-doped silica waveguides.² A number of similar four-port devices were subsequently proposed and demonstrated in both fiber and planar geometries (See, for example, Refs. 2 and 9–14). All the OADM device structures previously proposed and implemented have relied on DBR gratings fabricated by UV writing. The glass-integrated optic MZI OADM reported in this paper, however, exploits DBR technology with a sputter-deposited amorphous-silicon overlay for the first time, to our knowledge. A simplified method for overlay DBR fabrication, based on the low-temperature deposition of amorphous silicon and lift-off, is also established. The technical issues specific to the design, fabrication, trimming, and characterization of this device are studied and reported.

This paper is organized as follows. In Section 2 we present the design, fabrication, and optimization of an ion-exchanged glass waveguide MZI. We discuss details of high-index overlay DBR fabrication in Section 3. In Section 4 we report the measured performance of the MZI-OADM device. In Section 5 we present an alternative method for high-index overlay DBR fabrication. We summarize our results in Section 6.

2. Implementation of a Waveguide Mach-Zehnder Interferometer

Ion-exchanged waveguides in glass substrates have been used to demonstrate a variety of passive¹⁴ and active^{1,15} integrated optic devices. The waveguiding properties depend on the host glass and the ion-exchange process. For the work reported here we utilized an $\text{Ag}^+ - \text{Na}^+$ ion exchange and a silicate glass substrate. When compared with a $\text{K}^+ - \text{Na}^+$ ion exchange, the $\text{Ag}^+ - \text{Na}^+$ process produces a higher index contrast at shorter exchange times and lower processing temperatures.¹⁶ Silicate glass substrates offer better waveguide surface quality than phosphate glasses after lithography and etching processes have been performed. Thus silicate glass is preferred for passive applications that do not require the enhanced emission and absorption cross sections that are achievable with rare-earth-doped phosphate glasses. Among the variety of possible OADM structures, we chose the MZI-type implementation for two reasons. First, this implementation does not utilize intermodal coupling, and thus design and fabrication of the device are simpler. This is especially true when a high-index overlay is involved. More impor-

tant, the absolute position of the DBR along the interferometer arms does not affect device performance. Thus the MZI and DBR can be fabricated and tested separately. This separation offers significant advantages when different lithographic processes must be used to fabricate the waveguide and the DBR. In other OADM structures such a separation is not possible because of the high degree of interaction between the DC and the DBR.¹¹

Since a waveguide MZI is basically made of two cascaded 3-dB DCs, the DC characteristics significantly affect the performance of the resultant MZI OADM.¹² Each DC must have a split ratio of 50:50 in order that the passed signal appear only at the desired output port D. Any deviation from this split ratio results in leakage of the signal at port C. The length and separation between waveguides in the DC interaction region are the two main design parameters that determine the coupler's characteristics. In addition the bending loss due to the S bends of the DC is also an important factor. We used a commercially available propagation simulation program, based on the finite-difference beam propagation method (FD BPM), to find a coupler interaction length and a spacing value that yields a 50:50 split ratio.¹⁷ The program was also used to estimate the radiation loss from the S bends as a function of the bend radius. To obtain the waveguide index profiles for purposes of simulation and design, we first reconstructed the profiles of planar waveguides fabricated with high concentration melts by using the inverse-WKB method. The prism-coupling method was used to obtain the required effective indices.¹⁸ For most combinations of melt concentration and exchange time the reconstruction resulted in near-Gaussian refractive-index profiles. The empirical relations between the exchange parameters (concentration, temperature, duration) and the resulting waveguide characteristics (depth and index contrast) were used to crudely predict the refractive-index profile of a weakly guiding channel waveguide fabricated with a low-concentration AgNO_3 melt.

The prediction corresponded to a two-dimensional Gaussian profile with a $1/e$ depth of $3 \mu\text{m}$, a $1/e$ width of $6 \mu\text{m}$, and a peak index contrast at the air-glass surface of 0.03. Based on this mode profile and FD-BPM simulations, we set the S-bend radius of curvature, the waveguide separation, and the coupler interaction length of the DCs at 5 cm, $7.65 \mu\text{m}$, and 1 mm, respectively. The simulation predicted a 0.03-dB loss from each S bend. The MZI OADM was 3 cm long and had a port separation of $310 \mu\text{m}$, as indicated in Fig. 1. Since we lacked precise data of the waveguide index profile, it was not possible to design the MZI perfectly, or could we compare the resulting MZI performance with theory. Rather we chose to implement an approximate design and trim the device by using subsequent thermal annealing steps to achieve the desired performance (i.e., a 50:50 splitting ratio for the directional couplers). The availability of accurate data of the waveguide refractive-index profile, as could be obtained with a

refractive-near-field instrument, would improve the design step and reduce, or possibly eliminate, the need for postfabrication trimming.

Nine MZIs were fabricated on a single glass substrate by standard lithographic procedures and a Ti mask with 3- μm -wide MZI waveguide-channel openings. The substrate was subsequently immersed in a melt consisting of 0.25 mol.% AgNO_3 and 99.75 mol.% NaNO_3 at 320 $^\circ\text{C}$ for 20 min. After this ion-exchange step we removed the mask and diced and polished the sample. The completed MZIs were characterized for the degree of leakage at port C and total throughput. The measured power ratios of the passed signal at port D relative to the leakage at port C (i.e., the D/C power ratio) can be found in the last row of Table 1. A higher D/C ratio indicates a more balanced (i.e., closer to 50:50) operation of the DC. The total throughputs reported in Table 1 are informative only in a relative sense, because the input coupling loss and the output collection efficiency, which are hard to estimate, strongly affect these results. Furthermore input and output coupling was accomplished with bulk optics rather than by fiber pigtailing. After the ion-exchange step alone the D/C ratio was below unity, which indicated that the DCs were not well balanced. To improve DC performance, we annealed the sample for 20 min at 320 $^\circ\text{C}$.¹⁹ As indicated in Table 1, the annealing increased the D/C ratio to nearly 20 dB. A waveguide propagation loss below 0.4 dB/cm was inferred by finesse measurements of a ring resonator with a 2-cm diameter fabricated in the same substrate with the same process parameters. Following ion exchange, annealing, and characterization steps, we proceeded to the overlay DBR fabrication.

3. Fabrication of an Amorphous-Silicon Overlay Distributed Bragg Reflector

As mentioned in Section 1 the high-index overlay technique enables implementation of DBRs on hard-to-etch waveguide surfaces or on substrates that are not UV photosensitive. Furthermore it is a promising technology for devices controlled by electro-optic, thermo-optic, or nonlinear optical means. The presence of the overlay serves to load the surface of the underlying waveguide, and this loading locally modifies the effective index of the mode. Thus a periodic patterning of the overlay produces a periodic modulation of the effective index of the mode that results in distributed Bragg reflection. Figure 2 illustrates schematically the structure and waveguiding characteristics of a high-index overlay–waveguide compared with those of a waveguide without an overlay. The overlay material is usually chosen to have a much higher refractive index than the effective index of the unperturbed (i.e., without overlay) waveguide mode. As indicated in Fig. 2 the presence of the high-index overlay draws the mode into the overlay material, thus enhancing its interaction with the surface corrugation. This enhancement permits fabrication of short high-reflectivity DBR structures. In general the effective indices of the fundamental TE

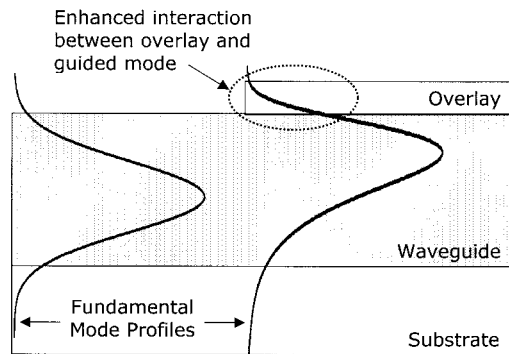


Fig. 2. Schematic diagram of the overlay–waveguide structure showing enhanced interaction between the overlay and the guided mode. The enhancement can improve the DBR reflectivity after a grating on the overlay is patterned.

and TM modes differ slightly, and thus the center wavelength of their corresponding drop bands also differs. Of more significance, however, is the fact that the modal interaction with a corrugated waveguide surface is much stronger for the TE than the TM modes.²⁰ Thus the drop band of the resulting overlay DBR device is polarization sensitive, and the efficiency with which the TM mode is dropped is very low. Figure 3(a) illustrates a method of fabricating a high-index overlay DBR in which the overlay material is deposited on the waveguide surface first and then lithographically patterned and subsequently etched to produce the corrugation. Figure 3(b) shows a slightly different method based on the lift-off that is described in Section 5. The OADM reported here was fabricated by using the procedure outlined in Fig. 3(a). A detailed analysis of the mode structure of the combined overlay/waveguide and corresponding design issues can be found in Refs. 7, 21, and 22. These studies demonstrate that the complex effective index of the mode, associated with

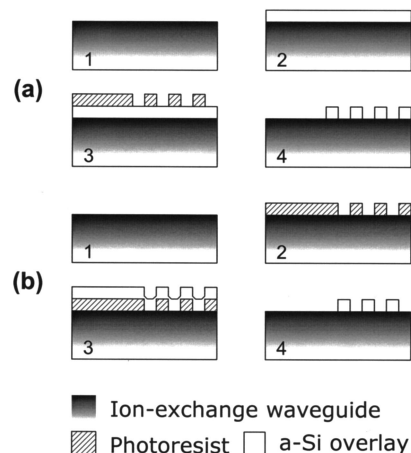


Fig. 3. Overlay DBR fabrication procedures: (a) Conventional: 1, ion exchange; 2, a-Si overlay deposition; 3, PR grating patterning; 4, pattern transfer to the overlay by RIE. (b) Lift-off: 1, ion exchange; 2, PR grating patterning; 3, a-Si deposition; 4, PR grating removal.

Table 1. Change in Waveguide MZI Characteristics at Each Fabrication Step

Characteristic Quantities	After					
	Step 1 Ion Exchange	Step 2 Annealing	Step 3 Deposition 1 (4.5 min)	Step 4 Deposition 2 (20 s)	Step 5 Deposition 3 (20 s)	Step 6 DBR fabrication
Relative throughput (%)	8.15	10.54	9.30	8.60	6.82	7.92
Overlay (or DBR) Induced loss per 1 cm (dB)	—	0 dB	0.54 dB	0.88 dB	1.89 dB	1.24 dB
D/C ratio	0.86	94.81	—	—	—	112.14

the combined overlay/waveguide structure, is a non-linear function of the overlay thickness. Up to a point the DBR reflectivity increases with overlay thickness. If the overlay material exhibits optical absorption, however, the imaginary part of the mode effective index grows as well, introducing loss into the device. Furthermore, beyond a certain overlay thickness, a majority of the mode power is confined in the overlay itself rather than in the underlying waveguide structure, resulting in a useless device. Based on these observations, the thickness T_0 of the overlay should be chosen to achieve a reasonable compromise between the induced propagation loss and the DBR reflectivity computed in the absence of loss.⁷ In the vicinity of T_0 losses increase rapidly with overlay thickness. Thus the overlay thickness must be controlled to near nanometer accuracy. An iterative deposition/measurement method that can be used to achieve this level of accuracy was described in Ref. 7. The effectiveness of the technique was proven by the successful realization of an Er/Yb co-doped waveguide laser array with overlay DBRs reported in the same paper.

In our previous overlay DBR laser work the overlay material was hydrogenated amorphous silicon deposited by PECVD. In the present work we chose to use amorphous silicon (a-Si) deposited by sputtering. As described in Ref. 7 sputter-deposited a-Si exhibits a higher optical loss due to absorption from silicon dangling bonds and scattering due to the inhomogeneities in the density of the film. For Ag-exchanged waveguides, however, the deposition process temperature becomes an important factor. Since the waveguides were fabricated in less than 20 min by Ag exchange at 320 °C, their index profiles would be significantly modified during a high-temperature (200–300 °C) PECVD process. For this reason a-Si deposited by a low-temperature (~80 °C) sputtering process was chosen. We used an Enerjet sputtering machine with the chamber pressure, the argon flux, the plasma power, and the planetary rotation rate maintained at 5×10^{-6} Torr, 34.1 sccm, 800 W, and 20 rpm, respectively. The overlay was deposited as a 1-cm-wide strip over the MZI arms. The complex refractive index of the deposited a-Si was measured to be $2.93 + i0.0048$ near 1550 nm with the technique described in Ref. 7.

For the OADM reported here we aimed to achieve >95% DBR reflectivity (computed in the absence of

loss), while limiting the 1-cm-long overlay DBR-induced loss to less than 1.5 dB. In Ref. 7 we reported a detailed description of the procedure needed to determine the optimum overlay thickness by relating the overlay-induced loss and the changes in the mode effective index. Implementation of this procedure required knowledge of the complex refractive index and the waveguide's refractive-index profile. Since the exact waveguide-index profile was not known, we approximated it as a one-dimensional Gaussian profile by using the $1/e$ depth specified in Section 2. The results of the one-dimensional modal analyses based on the transfer matrix method²³ indicated that a 2-dB/cm overlay-induced loss would correspond to a 1-cm-long overlay DBR having 90–99% reflectivity (computed in the absence of loss). Owing to our imprecise knowledge of the profile of the ion-exchanged waveguide refractive index, we set the duration of the first deposition conservatively and tried to approach the target overlay thickness with short additional depositions.

Table 1 shows the increase in overlay-induced loss computed from the measured decrease in the device throughput after successive deposition steps. Note that the third 20-s deposition step increased the overlay-induced loss by almost 1 dB, whereas the 4.5-min-long first deposition step resulted in only a 0.54-dB increase. From the data it was evident that we had entered the regime where the modal characteristics change as a function of overlay thickness very rapidly after the third deposition step.^{7,21,22} Thus we stopped deposition at this point. Using the calibrated deposition rate, we estimated that we had achieved an overlay thickness of ~25 nm. On completing the overlay deposition, we proceeded to fabricate a photoresist (PR) grating pattern and transferred this pattern into the overlay by reactive ion etching (RIE). The technical details of this procedure were the same as those reported in Ref. 7. Figure 4 is a top-view scanning electron microscope picture of an a-Si overlay DBR fabricated on an Ag-exchanged waveguide. The horizontal lines that appear at the waveguide edges are residue resulting from incomplete removal of the titanium mask used during the ion exchange. As indicated in Table 1 the 1-cm-long overlay DBR induced an additional loss of 1.24 dB. Note that we expect that the overlay DBR-induced loss would be one half of that of the overlay loss alone, since the duty cycle of the grating is ap-

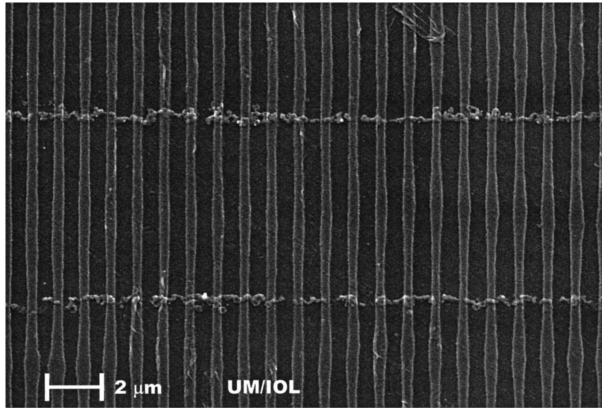


Fig. 4. Top-view SEM picture of an a-Si overlay DBR.

proximately 50%. The fact that the DBR overlay loss is higher than predicted can be attributed to scattering caused by the grating. A similar result was reported in Ref. 7. The data in Table 1 indicate that the completed device had a D/C power ratio of approximately 20 dB, which is almost the same value obtained from the MZI alone before the overlay was deposited.

4. Performance of the Optical Add-Drop Multiplexer

The MZI OADM was completely characterized following the fabrication. The OADM's spectral characteristics were obtained by using TE-polarized light from the source of amplified spontaneous emission as an input to port A and subsequently by scanning the device throughput from port D with an optical spectrum analyzer (OSA). The resolution of the OSA was 0.07 nm. The scanned transmission dip due to the DBR is shown in Fig. 5. The 24-dB transmission dip had its center wavelength at 1550.11 nm with a 3-dB bandwidth of 0.5 nm. The absence of multiple dips due to higher-order modes indicated that the overlay DBR did not perturb the single-mode nature of the waveguide.

Because the transmission dip scan of the amplified spontaneous emission gives only indirect information on the dropped signal, we set up an experiment to

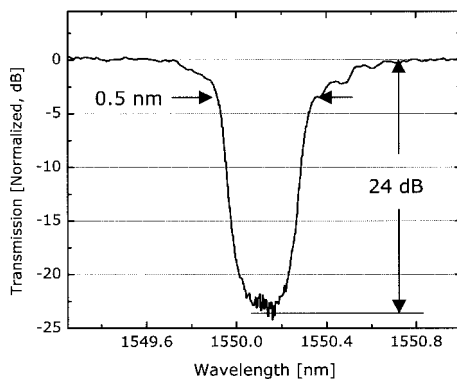


Fig. 5. Transmission dip of the completed MZI OADM with an overlay DBR.

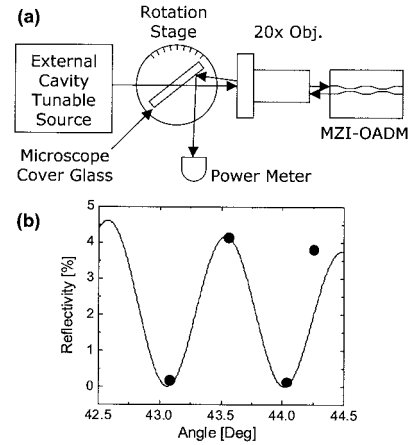


Fig. 6. (a) Experimental setup for drop-efficiency measurement. (b) Measured power of dropped signal fitted to a FP reflectivity curve as a function of the incidence angle.

measure directly the power of the dropped signal. Figure 6(a) shows the measurement setup. This time we used an external-cavity diode laser tuned to the DBR center wavelength as the input and a 150- μm -thick microscope cover glass to redirect the dropped signal onto a detector. We minimized the Fresnel loss of the incident beam at the cover glass by setting the incidence angle close to Brewster's angle. We were still able to measure the power of the dropped signal reflected off the cover glass because the dropped signal impinges on the microscope cover glass at an angle slightly deviated from Brewster's angle as illustrated in Fig. 6(a). One source of uncertainty in estimating the drop-efficiency signal power from the reflected power is the dependence of the cover-glass reflectivity on incidence angle. Since the 150- μm -thick microscope cover glass effectively becomes a Fabry-Perot (FP) cavity when reflecting a 1550-nm beam, its reflectivity is an oscillating function of the incidence angle. We used the well-known FP reflectivity formula to calculate the TM-input reflectivity R_{TM} of a FP cavity. The plot in Fig. 6(b) shows the rapid changes of R_{TM} for a 150- μm -thick cover glass with an index of 1.51 at 1530 nm as a function of incidence angle θ . Even after the rapid variation in R_{TM} was identified, the high sensitivity of R_{TM} to θ still caused uncertainty due to small errors in angle measurement and alignments.

To overcome this problem, first we scanned an angular range that contained three to four maxima and minima of R_{TM} by rotating the stage upon which the cover glass was mounted. We fit these results to the theoretical FP reflectivity curve. The measurement results are marked as dots in Fig. 6(b). At around $\theta = 43.5^\circ$ where the FP R_{TM} reaches the local maximum of 4.3%, we measured a drop efficiency of 8.2%. The measured drop efficiency, when compared with the 7.92% throughput value in the last column of Table 1, indicated that the insertion loss from port A to D (pass mode) was nearly equal to that from port A to B (drop mode). Note that bulk optics were used to

couple into and out of the device, and thus the throughput values reported in Table 1 are not representative of the values that would be achieved with fiber-to-device coupling.

Comparisons with other MZI OADM are useful for assessing device performance. In Refs. 2 and 13 two such devices are reported. In Ref. 2 Kashyap *et al.* fabricated a UV-written MZI OADM in a photosensitive Ge-doped planar silica substrate. After the UV-trimming process the completed device exhibited a 3-dB transmission dip 15 dB deep, 1 nm wide from a 2-mm-long grating. The D/C ratio was approximately 3.7%, and the fiber-to-fiber insertion loss was 1.35 dB. In Ref. 13 a device is reported with a similar structure and fabrication method. The resultant device after UV trimming showed a 3-dB transmission dip 36 dB deep, 1.1 nm wide from a 3.8-mm-long grating. The length of the device was 25 mm, the fiber-to-fiber insertion loss was approximately 1 dB, and the D/C ratio was approximately 10%. Compared with these results, our device exhibited a generally higher insertion loss (i.e., 2.5 dB excluding input/output coupling), a better D/C ratio, and comparable transmission dip characteristics.

MZI OADM fabricated by direct UV exposure often require trimming the interferometer to compensate for nonidentical UV-induced gratings in the two arms.¹² The overlay DBR grating technique appears to be more robust in this regard, since it is easier to make the gratings in the two arms identical. The overlay DBR suffers, however, from the serious problem of polarization sensitivity, but an overlay DBR may be the only option when other considerations require use of a non-UV-photosensitive substrate.

5. Overlay Distributed Bragg Reflector Fabrication by Lift-off

When the overlay material can be deposited at low temperatures, as is the case for the sputter-deposited a-Si, it is possible to fabricate the overlay DBR by a lift-off technique. This lift-off fabrication procedure is illustrated in Fig. 3(b). By directly using the PR grating as the lift-off mask, we were able to eliminate the RIE pattern transfer step. This lift-off technique cannot be used for materials deposited by PECVD due to outgassing from the PR at high temperatures.

As the first step we made a PR grating on a K^+Na^+ ion-exchanged waveguide by using the same procedure described in Section 3. Since the PR grating functioned as the mask for lift-off in this work, special attention was paid to the duration of the postbake step and the safe lift-off of the PR grating after the overlay deposition. In our experience 10 min of postbake at 130 °C hardened the PR grating sufficiently to allow it to withstand bombardment of sputtered a-Si in the conditions specified in Section 3. After the postbake we proceeded to a-Si sputtering. Although the sputtering-process parameters were the same as reported in Section 3, it was difficult to

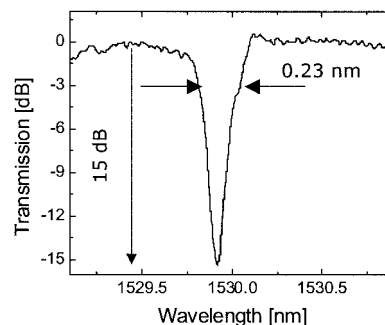


Fig. 7. Transmission dip of an a-Si overlay DBR fabricated by the lift-off technique.

estimate the deposition thickness because of the presence of the 150-nm-thick PR grating.

Since the iterative technique of deposition followed by a throughput measurement was not applicable to this structure, we had to make several DBRs with different deposition times to obtain a satisfactory DBR response. Before characterizing the device, we removed the PR grating by placing the sample for 30 min in a cold acetone bath followed by scrubbing it with acetone-drenched cotton swabs. We avoided the use of a hot acetone bath so as not to remove the sputtered a-Si itself. With an 8.5-min long deposition we obtained a spectral response comparable with that reported in Section 4. Figure 7 shows an OSA scan of the transmission dip obtained from a throughput measurement. The 15-dB dip had a 3-dB bandwidth of 0.23 nm. The overlay DBR-induced loss was measured to be 1.15 dB/cm and was approximately the same as that reported in Section 4. The lift-off technique is simple and fast and thus may prove useful for fast prototyping of overlay DBR waveguide devices.

6. Conclusions

In summary, we report the fabrication of a distributed Bragg reflector (DBR) on an ion-exchanged glass waveguide by using a patterned overlay of sputter-deposited amorphous silicon (a-Si). Using a high refractive-index overlay DBR, we have demonstrated a fully functional glass-integrated optic add-drop multiplexer (OADM), thus illustrating the applicability of the overlay grating technology for hard-to-etch or non-UV-photosensitive substrates. The 3-cm-long OADM consisted of a Mach-Zehnder interferometer containing overlay DBR gratings in both arms. The MZI was fabricated in a silicate glass substrate by a low-concentration silver ion exchange. We successfully utilized thermal annealing to trim the directional couplers in the MZI, obtaining the desired 50:50 split ratio. The completed glass waveguide MZI had a propagation loss of less than 0.4 dB/cm. We implemented the DBR by patterning and etching a 25-nm-thick a-Si overlay sputter deposited on the top of the waveguide MZI. An iterative deposition technique played an essential role in finding and achieving an appropriate overlay thickness. The

completed glass waveguide MZI OADM exhibited a 24-dB transmission dip with a 0.5-nm 3-dB bandwidth at 1550.11 nm. The 1-cm-long overlay DBR-induced loss was approximately 1.24 dB.

A direct measurement of dropped signal power indicated that the device throughput was the same when it was operated in either the pass or drop state. A simplified overlay DBR fabrication method based on the lift-off technique was also proposed and demonstrated. An overlay DBR fabricated with this technique exhibited a 15-dB transmission dip with a 0.23-nm 3-dB bandwidth. Based on size, performance, and ease of fabrication, the high-index overlay technique shows the potential for applications that require implementation of DBR gratings in non-photosensitive glasses or difficult-to-etch substrates. The main limitation of an overlay DBR is its polarization sensitivity. Corrugated surface gratings, as opposed to UV-induced intracore gratings, are highly polarization sensitive, exhibiting very low reflectivity for the TM mode. Thus overlay DBR-based devices need to be monolithically integrated with other polarization-controlling components, such as polarizers and rotators, for polarization-insensitive operation to be realized.

References

1. J. E. Roman and K. A. Winick, "Neodymium-doped glass channel waveguide laser containing integrated distributed Bragg reflector," *Appl. Phys. Lett.* **61**, 2744–2746 (1992).
2. R. Kashyap, G. D. Maxwell, and B. J. Ainslie, "Laser-trimmed four-port bandpass filter fabricated in single-mode photosensitive Ge-doped planar waveguide," *IEEE Photonics Technol. Lett.* **5**, 191–193 (1993).
3. C. P. Hussell and R. V. Ramaswamy, "High-index overlay for high-reflectance DBR gratings in LiNbO_3 channel waveguides," *IEEE Photonics Technol. Lett.* **9**, 636–638 (1997).
4. M. Zelikson, J. Salzman, K. Weiser, and J. Kanicki, "Enhanced electro-optic effect in amorphous hydrogenated silicon based waveguides," *Appl. Phys. Lett.* **61**, 1664–1666 (1992).
5. G. Cocorullo, F. G. Della Corte, R. De Rosa, I. Rendina, A. Rubino, and E. Terzini, "Amorphous silicon-based guided-wave passive and active devices for silicon integrated optoelectronics," *IEEE J. Sel. Top. Quantum Electron.* **4**, 997–1002 (1998).
6. R. M. Ribeiro, L. R. Kawase, W. Margulis, B. Lesche, B. Sahlgren, R. Stubbe, and K. Kleveby, "All-optical control of Bragg grating in semiconductor-coated D-shaped fiber," *Opt. Lett.* **24**, 454–456 (1999).
7. J. Kim, C. Florea, K. A. Winick, and M. McCoy, "Design and fabrication of low-loss hydrogenated amorphous silicon overlay DBR for glass waveguide devices," *IEEE J. Sel. Top. Quantum Electron.* **8**, 1307–1315 (2002).
8. D. C. Johnson, K. O. Hill, F. Bilodeau, and S. Faucher, "New design concept for a narrowband wavelength-selective optical tap and combiner," *Electron. Lett.* **23**, 668–669 (1987).
9. I. Baumann, J. Seifert, W. Nowak, and M. Sauer, "Compact all-fiber add-drop multiplexer using fiber Bragg gratings," *IEEE Photonics Technol. Lett.* **8**, 1331–1333 (1996).
10. A. S. Kewitsch, G. A. Rakuljic, P. A. Williams, and A. Yariv, "All fiber zero insertion loss add drop filter for WDM," *Opt. Lett.* **23**, 106–108 (1998).
11. C. Riziotis and M. N. Zervas, "Design considerations in optical add-drop multiplexers based on grating-assisted null coupler," *J. Lightwave Technol.* **19**, 92–104 (2001).
12. T. Erdogan, T. A. Strasser, M. A. Milbrodt, E. J. Laskowski, C. H. Henry, and G. E. Kohnke, "Integrated-optical Mach-Zehnder add-drop filter fabricated by a single UV-induced grating exposure," *Appl. Opt.* **36**, 7838–7845 (1997).
13. J. Albert, F. Bilodeau, D. C. Johnson, K. O. Hill, K. Hattori, T. Kitagawa, Y. Hibino, and M. Abe, "Low-loss planar lightwave circuit OADM with high isolation and no polarization dependence," *IEEE Photonics Technol. Lett.* **11**, 346–348 (1999).
14. D. F. Geraghty, D. Provenzano, M. M. Morrell, S. Honkanen, A. Yariv, and N. Peyghambarian, "Ion-exchange waveguide add-drop filter," in *Integrated Optics Devices V*, G. C. Righini and S. Honkanen, eds., *Proc. SPIE* **4277**, 85–190 (2001).
15. D. L. Veasey, D. S. Funk, N. A. Sanford, and J. S. Hayden, "Arrays of distributed-Bragg-reflector waveguide lasers at 1536 nm in Yb/Er codoped phosphate glass," *Appl. Phys. Lett.* **74**, 789–791 (1999).
16. S. Iraj Najafi, ed., *Introduction to Glass Integrated Optics* (Artech House, Norwood, Mass., 1992).
17. R. Scarmozzino, A. Gopinath, R. Pregla, and S. Helfert, "Numerical techniques for modeling guided-wave photonic devices," *IEEE J. Sel. Top. Quantum Electron.* **6**, 150–162 (2000).
18. R. Ulrich and R. Torge, "Measurement of thin film parameters with a prism coupler," *Appl. Opt.* **12**, 2901–2908 (1973).
19. R. Srivastava, H. Zhenguang, and R. V. Ramaswamy, "Effect of annealing of diffused channel waveguides," *Appl. Opt.* **29**, 330–331 (1990).
20. T. Tamir, ed., *Guided-Wave Optoelectronics* (Springer-Verlag, Berlin, 1988), Chap. 2.
21. R. F. Carson and T. E. Batchman, "Multimode phenomena in semiconductor-clad dielectric optical waveguide structures," *Appl. Opt.* **29**, 2769–2780 (1990).
22. T. Conese, R. Tavlykaev, C. P. Hussell, and R. V. Ramaswamy, "Finite element analysis of LiNbO_3 waveguides with Si or Si/SiO₂ overlay," *J. Lightwave Technol.* **16**, 1113–1122 (1998).
23. K.-H. Schlereth and M. Tacke, "The complex propagation constant of multilayer waveguides: an algorithm for a personal computer," *IEEE J. Quantum Electron.* **26**, 627–630 (1990).